Article

Resolving active species during the carbon monoxide oxidation over Pt(111) on the microsecond timescale

Calley N. Eads[1], Weijia Wang [1], Ulrike Küst [2,3], Julia Prumbs [2], Robert H. Temperton [1], Mattia Scardamaglia [1], Joachim Schnadt[1,2,3], Jan Knudsen[1,2,3] & Andrey Shavorskiy [1] ✉

Catalytic studies traditionally rely on steady-state conditions resulting in time-averaged datasets that do not differentiate between active and spectator species. This limitation can cause misinterpretations of catalytic function, as the signal of short-lived intermediates responsible for producing desired reaction products is often masked by more intense spectator species. Time-resolved ambient pressure X-ray photoelectron spectroscopy (tr-APXPS) mitigates this issue by combining microsecond time resolution under reaction conditions. Using tr-APXPS, we investigate the oxidation of CO over Pt(111) by concurrently tracking reaction products, surface intermediates, and catalyst response. Our findings reveal that chemisorbed oxygen, rather than Pt surface oxide, is the main species reacting with CO to form CO_2, supporting a primary Langmuir-Hinshelwood mechanism. The results shed new light on a heavily-debated reaction in catalysis. Beyond using CO pulses to determine active species, we demonstrate how careful tuning of pulsing parameters can be used for dynamic catalyst operation to enhance CO_2 formation.

The development of novel experimental methods enabling the study of materials and processes with higher complexity than before can significantly impact even well-established research areas, sometimes prompting a rethinking of existing theories. A classic example is the investigation of carbon monoxide oxidation over platinum-group metals. In the 1980s and 1990s, surface science experiments clearly supported the Langmuir-Hinshelwood (LH) mechanism, identifying chemisorbed oxygen as the sole reactive species[1–3]. However, with the advent of operando techniques in the 2000s, the study of catalytic reactions under (near) ambient pressures and technologically relevant temperatures provided evidence of platinum oxide formation, which sometimes correlated with enhanced catalytic activity[4–6]. These new operando findings led to a revision of the existing understanding of the CO oxidation mechanism, suggesting that platinum oxide is the catalytically most active species and that the oxidation proceeds through the Mars-van-Krevelen (MvK) mechanism[7,8]. However, other operando studies have found no evidence of platinum oxide formation[9–11] or suggested that platinum oxide plays only a spectator role[12–15], supporting the original LH mechanism with metallic platinum as the active site[16,17]. As it appears today, the mechanism of CO oxidation over platinum under (near) ambient conditions remains unresolved. Settling this debate requires developing advanced experimental capabilities that can explore new dimensions of the reaction, such as spatial or time resolution, in combination with operando capabilities[6,18,19]. We propose a time-resolved approach to differentiate active from spectator species in CO oxidation of Pt.

Most often, operando catalyst research is conducted under steady-state conditions, yielding time-averaged data that overlook the dynamic behavior of reaction species[18,20–22]. This approach can result in observational claims about the slowest reaction step[23] and the most abundant intermediates, which are not necessarily the active species[24,25]. To better understand the catalytic mechanism, it is

[1]MAX IV Laboratory, Lund University, Lund, Sweden. [2]Division of Synchrotron Radiation Research, Department of Physics, Lund University, Lund, Sweden. [3]NanoLund, Lund University, Lund, Sweden. ✉e-mail: andrey.shavorskiy@maxiv.lu.se

essential to track the exact sequence of surface transformations on a timescale comparable to that of the elementary reactions. This can be achieved by perturbing steady-state conditions with a rapid chemical potential change in the form of a gas or temperature pulse, triggering a collective response from all active sites. Time-resolved techniques then observe the synchronous evolution of surface species, effectively revealing the catalytic cycle directly[18,26,27].

The most relevant timescales for individual reaction steps are microseconds to milliseconds[18,19]. However, investigating the dynamics of surface elementary reactions on these timescales under pressure and elevated temperature conditions with high chemical specificity intact remains challenging. Leading time-resolved techniques include the temporal analysis of products (TAP)[28,29], molecular beam (MB)[30,31], steady-state isotopic transient kinetic analysis (SSITKA)[32,33], and modulation excitation spectroscopy (MES)[34,35] with phase-sensitive detection[27,36,37] or frequency space data analysis[38,39] (Supplementary Table 1). These methods use modulation parameters, such as rapid cycling of gas pressures, temperature, or concentration, and evaluate the catalytic activity based on gas phase products in mass spectrometry (MS). TAP and SSITKA offer second to sub-second resolution, while MB achieves microsecond resolution but is limited to $<10^{-3}$ mbar pressures. Nevertheless, gaining deeper insights into underlying surface processes requires coupling with spectroscopic or scattering tools, where time resolution is contingent upon the analysis technique (Supplementary Table 1). Since these methods are not typically event-averaged over many cycling events, their time resolution is limited by the signal-to-noise ratio of a single spectrum. Additionally, many MES techniques like X-ray diffraction (XRD) and X-ray absorption spectroscopy (XAS) are bulk sensitive, which limits their ability to analyze surface-active species that usually define catalytic function.

The importance of studying catalytic reactions under periodic cycling conditions extends beyond academic interest, as it has been experimentally shown to improve conversion rates in industrial CO and hydrocarbon oxidation on supported Pt and Pd catalysts[18,40–45] compared to steady-state flow regimes. For instance, automotive catalytic converters have an inherent modulation in the gas atmosphere due to a feedback loop that sets an effective air-to-fuel ratio in the exhaust gas, which constantly corrects fuel and air injections, creating rapid transient changes in gas composition. Researchers at Toyota and General Motors performed numerous experiments testing these modulation parameters on real catalysts under practical conditions and found differences in product formation[41,45]. These processes are vital for emission control and hydrogen purification, with significant economic and regulatory implications[46]. These discoveries have spurred further research into the periodic or "unsteady-state" operation of catalytic converters and other technologies, showing immense success compared to their steady-state alternatives[24,47–49]. The rate acceleration of catalytic processes induced by oscillating the catalyst between two electronic states is also the theoretical basis of surface resonance theory[50]. While redesigning existing technologies to include periodic operation is appealing[51–53], the chemical transformations driving higher conversion rates are not yet fully understood. Advancement first requires studying underlying phenomena under relevant reaction conditions using analysis techniques with adequate time resolution.

We have recently established a time-resolved ambient pressure X-ray photoelectron spectroscopy (tr-APXPS) methodology[54–56] to tackle these challenges by concurrently tracking the evolution of surface intermediates and gas phase contributions with microsecond time resolution using chemical perturbations operating at near ambient pressures and elevated temperatures[56]. This powerful method clearly separates active and spectator species by modulating conditions and directly linking them to gas phase products, probing chemical dynamics in any reversible catalytic reaction. In this work, we revolutionize the method by integrating a delay-line detector (DLD) in the

spectrometer, enabling us to continuously (i.e., throughout the entire cycle) monitor the surface and gas phase evolution with high time resolution. We stress that with the introduction of the DLD, such information can be obtained for all time delays from a single measurement. This starkly contrasts with previous measurements[56] where a single time delay could be obtained per one measurement. By introducing the DLD in this work, it was possible to increase the data collection efficiency by one to two orders of magnitude[26], allowing for a level of detail previously impossible to obtain. For example, with the new detection scheme, we could clearly identify the part of the catalytic cycle where a highly active phase transitions into a phase with low activity, pinpointing the precedence of a specific mechanism.

In this work, we studied the time evolution of reaction species in the CO oxidation of Pt(111) at 333 °C by periodically modulating CO gas into an O_2 stream and capturing chemical transformations with 40 μs resolution. Within this timeframe, we assess active and spectator species. We find that chemisorbed oxygen, O_{chem}, plays a critical role in CO_2 production while oxygen species in the oxide, O_{oxide}, mostly spectates. Our results support a primary LH mechanism with active O_{chem} species and a secondary MvK mechanism involving less reactive O_{oxide}. Through this understanding of the structure-activity relationship, we explore how varying CO pulsing parameters can toggle CO_2 production on and off, enabling control of reactivity.

Results

Time-resolved methodology

Contrary to a typical reactor scheme that utilizes a continuous flow of all reactant gases, our tr-APXPS set-up pulses one reactant gas (CO) into a continuous stream of a different reactant gas (O_2) while observing time-dependent chemical composition changes via XPS using a 2D delay-line detector (DLD) (Fig. 1a). Synchronization of the gas pulses with the DLD via a function generator provides the platform to directly obtain 2D plots (maps) of kinetic energy vs. time during the duration of each gas pulse (Fig. 1b, step 1). The normal photoelectron spectrum is then reconstructed from multiple such time-resolved measurements with the kinetic energy swept between each of them (Fig. 1b, step 2). This is repeating a well-known swept mode of acquisition, the most common way of recording XPS. The key to the set-up is the aforementioned hardware synchronization, which ensures the timing structure within the 2D maps to be exactly the same allowing averaging of the time-resolved data between numerous pulses (Fig. 1b, step 3). Pertinent to our current study monitoring CO oxidation over Pt(111), Fig. 1b presents a 2D plot of C $1s$ gas phase when pulsing CO gas at 10 Hz into an O_2 stream averaged over 90,000 pulses taking 2.5 h. Integrating over the CO gas phase feature reveals the profile of the CO gas pulse with pulsing regions that are commonly referred to throughout the text. Briefly, before the pulse is the delay between the data acquisition start time and the CO(g) signal. The rising edge begins when the CO pulse reaches the sample and ends with CO(g) equilibration. On-pulse denotes when CO(g) is constant. The falling edge begins when CO is pumped out, reducing the CO(g) signal.

Microsecond compositional changes during CO oxidation over Pt(111)

We employ tr-APXPS to uncover mechanistic information involving both surface and gas phase species when pulsing CO at 10 Hz (100 ms period) into a stream of O_2 (see Methods for experimental details). Figure 2 shows time-resolved 2D plots of XPS data of relevant core levels (top panel), and representative fits (bottom panel) at certain time points (I–IV) along the CO pulse (top left). The CO pulse profile derives from the CO(g) component of C $1s$ gas phase spectra (Fig. 2a) and is divided into four regions: (1) before pulse (<0 ms, light gray), (2) rising edge (0.0–1.6 ms, burgundy), (3) on-pulse (1.6–2.8 ms, red), and (4) falling edge (>2.8 ms, dark gray). Note that gas phase (GP) spectra were recorded 450 μm from the normal XPS position to
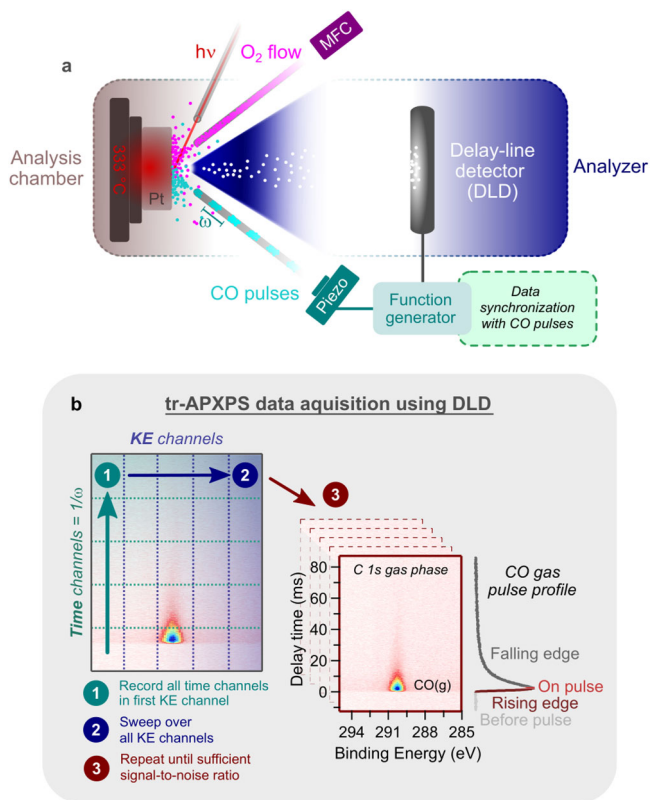
Fig. 1 | tr-APXPS experimental set-up with data acquisition flow using a 2D delay-line detector. a O_2 and CO gases are separately introduced facing a Pt(111) crystal in the analysis chamber. O_2 flow is set by a mass flow controller (MFC) and CO is pulsed at a specific frequency ω, using a piezo valve synchronized to a delay-line detector (DLD) via a function generator. Using this set-up, event-averaged 2D plots of XPS data with a time axis defined by the pulsing frequency ($1/\omega$) are obtained. **b** Simplified visualization of tr-APXPS data acquisition where each time channel is measured at one kinetic energy (KE) channel before sweeping over another kinetic energy channel and measuring all time points. This procedure repeats until all kinetic energy channels are measured. Data collection continues as described until a sufficient signal-to-noise ratio is reached as defined by the user. An example 2D plot of the C 1s gas phase is presented with a side view of the CO pulse profile detailing regions of interest.

probe only gas phase molecules. Surface transformations induced by the CO pulse are evident in these 2D plots (Fig. 2a–e) and lead to increases in CO_2 production. For instance, Fig. 2c shows O adsorbates quickly replaced by CO adsorbates (CO_{ads}) after the CO pulse (~0 ms) and a gradual return to an O-covered surface when CO is pumped away (30–40 ms).

To assess surface changes linked to enhanced CO_2 production, tr-APXP line spectra were extracted, averaged accordingly to achieve a reasonable signal-to-noise ratio within each region, and fitted (Fig. 2f–j; see Methods). The fitted binding energies match well with the literature values (Supplementary Table 2). Figure 3 compares fitted areas at incremental time steps across the CO pulse to provide a comprehensive view of the reaction mechanism and enable the determination of active species driving CO_2 production by directly correlating gas phase product formation with surface changes (Fig. 3).

The O *1s* GP signals in Fig. 3a illustrate the response of both reactants (CO, O_2) and products (CO_2); these are found to be in line with the C *1s* GP signals (Supplementary Fig. 2). CO_2 forms immediately after CO is introduced, persists for 480 µs, then abruptly stops. As CO levels diminish on the falling edge, CO_2 production resumes after 2 ms and peaks after another 26 ms (IV), before it gradually declines over the falling edge. To understand these changes, we analyze the

response of the surface species—carbon and oxygen adsorbates—and the Pt catalyst.

In Fig. 3b, the C *1s* areas show an absence of carbon adsorbates before the pulse, followed by the rapid growth of CO adsorbates (CO_{ads}) in two different configurations: CO bonded to one (CO_{top}) and two (CO_{bridge}) Pt atoms on the rising edge. CO_2 formation closely correlates with an increase in CO_{ads} intensity on the rising edge of the pulse until saturation is reached after 400 µs. During the rest of the rising edge and the on-pulse region, CO_{top} and CO_{bridge} species remain relatively stable, with CO_{top} at 61% of the total CO intensity (III). On the falling edge, CO desorption creates free sites for O_2 dissociation and subsequent reaction, triggering CO_2 production that peaks at IV, where the CO_{ads} concentration is minimal and primarily composed of CO_{top} (76%). The remainder of the falling edge continues to exhibit CO_2 production, but without CO_{ads} signal being visible due to the low residence time of CO on the surface (likely less than thermal CO desorption at a few hundred µs[57]): surface-bonded CO reacts instantaneously with O adsorbates to form CO_2.

In Fig. 3c, O *1s* areas trend shows both CO_{ads} and O adsorbates signal with matching CO_{ads} trends from the C *1s* spectra (Fig. 3b). Prior to the CO pulse, the surface is covered by chemisorbed oxygen (O_{chem}) and Pt surface oxide (O_{oxide}). When CO is introduced on the rising edge of the pulse, O_{chem} and O_{oxide} are rapidly, within ~400 µs, replaced by CO_{ads}, creating a CO-covered surface. During this initial oxygen-rich phase, CO_2 production is high, indicating a highly catalytically active mixed O_{chem}–O_{oxide} phase. Looking more closely at the time evolution of the two oxygen species shows that O_{oxide} consumption is slightly delayed (120 µs) with respect to that of O_{chem}. As CO_{ads} accumulate, the surface becomes poisoned, which hinders oxygen dissociation. This effect is reversed on the falling edge as CO gas is pumped away, reducing the CO_{ads} equilibrium coverage and allowing oxygen to dissociate, forming O_{chem} and O_{oxide}, which correlates with increased CO_2 production. Notably, the O_{oxide} intensity increases significantly during the initial 34 ms of CO desorption/32 ms of CO_2 production, while the small amount of O_{chem} intensity only markedly increases after CO_2 production peaks and O_{oxide} stabilizes (red dashed box). The delayed increase of O_{chem} intensity compared to that of O_{oxide} during the falling edge mirrors the trends seen during the rising edge, suggesting a similar mechanism. This key observation implies that O_{chem} plays an active role in CO oxidation, a point further explored in the "Discussion" section.

In Fig. 3d, the Pt $4f_{7/2}$ intensity trends demonstrate the response of the Pt catalyst. These reflect trends similar to those seen for the CO_{ads}, O_{chem}, and O_{oxide} components in the O *1s* spectra. On the rising edge, O_{chem} reacts at a higher rate than O_{oxide}, a pattern mirrored on the falling edge, consistent with the above O *1s* observations. Further analysis of the Pt $4f_{7/2}$ intensities shows an unexpected increase in coordinately unsaturated Pt atoms (Pt_{surf}) as O adsorbates are removed, implying exposed areas of bare metallic Pt. The Pt_{surf} intensity peaks when O_{chem} is fully consumed after 280 µs. At this stage, the remaining O_{oxide} is consumed, and CO_{ads} build on the surface with the depletion of Pt_{surf}. At CO_{ads} saturation, Pt_{surf} signal declines exponentially, potentially a result of slow Pt atom diffusion originating from Pt atoms/clusters that are left behind when CO_{ads} react with oxygen atoms in O_{oxide}. Moreover, CO_{bridge} signal increases as Pt_{surf} signal decreases from 0.4–0.8 ms, suggesting that CO molecules are preferentially adsorbing in a bridged configuration as Pt sites become available. Pt_{surf} signal continues to decline until ~1.2 ms but can be considered within the noise of the fit from 0.8–1.2 ms. This behavior repeats on the falling edge, with Pt_{surf} decreasing as O_{chem} builds up (after IV). Overall, tr-APXPS provides a comprehensive mechanistic explanation of gas phase and surface species dynamics throughout the CO oxidation reaction, allowing us to pinpoint periods of highest CO_2 production and understand the corresponding surface responses critical for its formation.
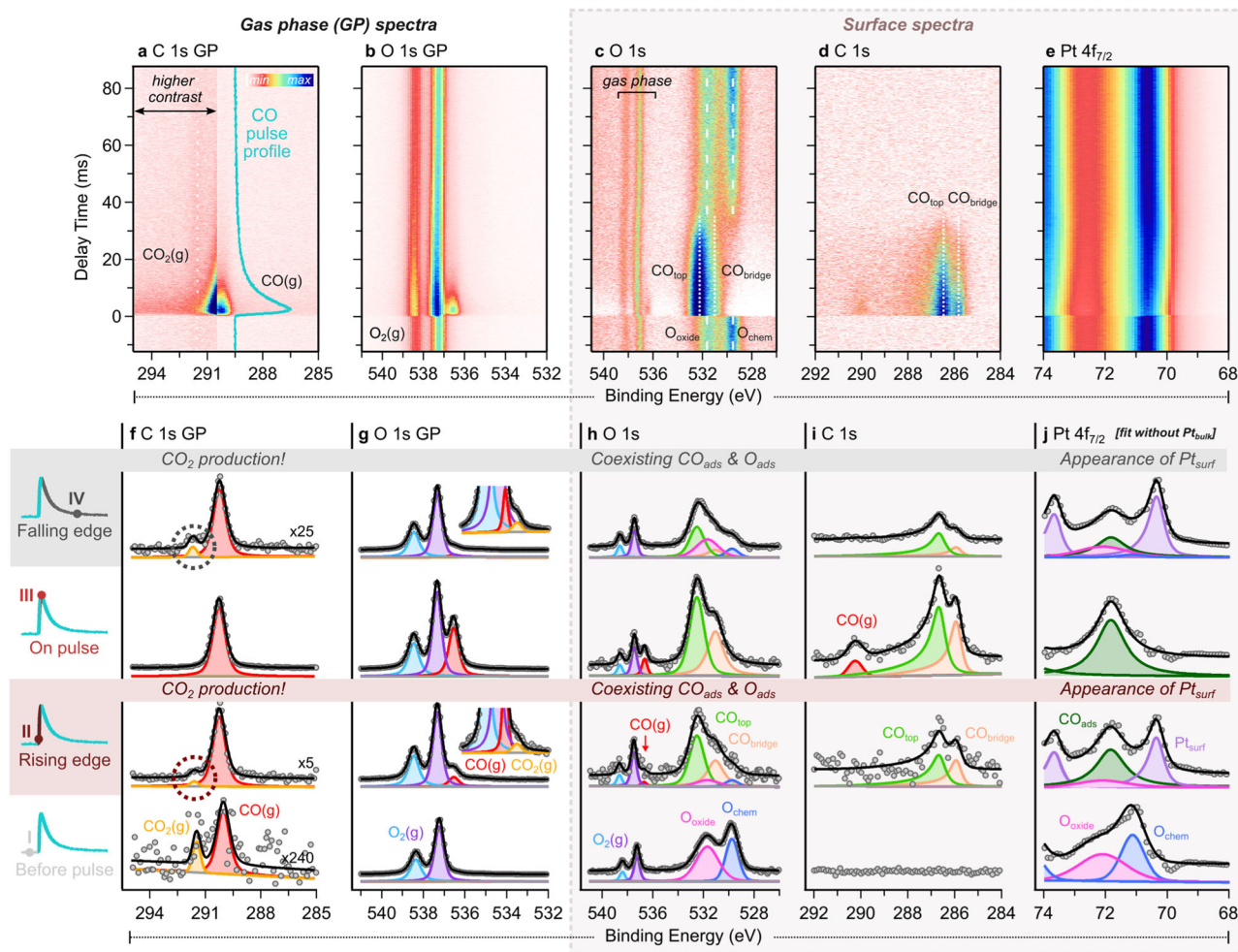
Fig. 2 | tr-APXPS data of CO oxidation over Pt(111) with 40 μs time resolution when pulsing CO gas at 10 Hz into a constant flow of O₂ gas while monitoring gas phase and surface core levels. 2D plots (top panel) and representative curve fit (bottom panel) at specific instances in time across the CO pulse as indicated by points I, II, III, and IV. Shown are the C 1s gas phase (GP) signal, at high binding energy displayed using a higher contrast region to amplify the faint $CO_2(g)$ feature (**a, f**), O 1s GP signal with insets magnifying CO(g) and $CO_2(g)$ when appropriate (**b, g**), O 1s (**c, h**), C 1s (**d, i**), and Pt $4f_{7/2}$ core levels (**e, j**). To accurately assess the Pt $4f_{7/2}$ fits (**j**), the Pt_{bulk} component was removed (see Supplementary Fig. 1 for the original fit with Pt_{bulk}). Each row of fitted spectra (I–IV) equates to a slice of time on the 2D plots and represents significant points along the CO pulse within each pulsing region, also denoted by dashed lines in Fig. 3.

Tuning catalytic activity with CO pulsing parameters

To further explore the CO oxidation mechanism, we focused on regions of high catalytic activity and inactivity by adjusting our pulsing scheme to mimic each independently. To target the peak reactivity region (IV in Fig. 3a), we tuned the pulsing parameters to aim at continuous CO_2 production resulting in pulsing CO at 50 Hz (Fig. 4). Increasing the pulsing frequency from 10 Hz to 50 Hz reduced the time window from 100 ms to 20 ms, leading to more gas overlap due to the limited pumping speed, resulting in the constant presence of CO. As shown in Fig. 4a, the C 1s GP spectra display continuous CO and CO_2 signals. The O 1s line in Fig. 4b mirrors the surface transformations seen at 10 Hz (Fig. 2c,h), with CO_{ads} and O adsorbates alternating in response to CO pulsing, driving CO_2 formation. Despite a lower signal-to-noise ratio, it is still possible to fit the O 1s and C 1s data in coarse time steps (1 ms/50 spectra) to track surface composition changes. Given the intensity of the CO_{ads} signal in the C 1s spectra (Fig. 4c), the C 1s GP and O 1s intensity trends in Fig. 4d highlight a preference for consumption of O_{chem} over that of O_{oxide} upon CO pulsing. Additionally, we observe a switch between CO_{top} and O_{chem}: initially, at the start of the pulse, intensities are low for CO_{top} and high for O_{chem}, but they become high for CO_{top} and low for O_{chem} after the pulse (Fig. 4d). This trend, reversed at 10 Hz on the falling edge in Fig. 3c, albeit with

different coverages, shows how 50 Hz targets the peak CO_2 production conditions seen at 10 Hz. This demonstrates the precision in controlling reactivity using CO pulsing parameters based on the structure-activity relationship.

Alternatively, we can adjust our pulsing parameters to deactivate the catalyst by extending the opening time of the CO pulsing valve to increase CO pulse pressure. CO_2 was not detected, and previous surface transformations in O 1s are no longer observed, replaced instead by a constant CO-rich environment (Supplementary Fig. 3). Comparison of traditional steady-state conditions to a modulating gas atmosphere also shows a level of reactivity control due to changes in surface interactions (Supplementary Note 1 and Supplementary Fig. 4).

Discussion

The results indicate that favorable conditions for CO_2 conversion occur within narrow periods during CO pulsing, as the system transitions through low-activity CO- and O-poisoned phases. These active periods of CO_2 production occur on the rising and falling edges (and during the 50 Hz experiment), where surface transformations expose bare Pt_{surf} areas, fostering reactive O_{chem} and CO_{ads} along with the formation of less reactive O_{oxide}.
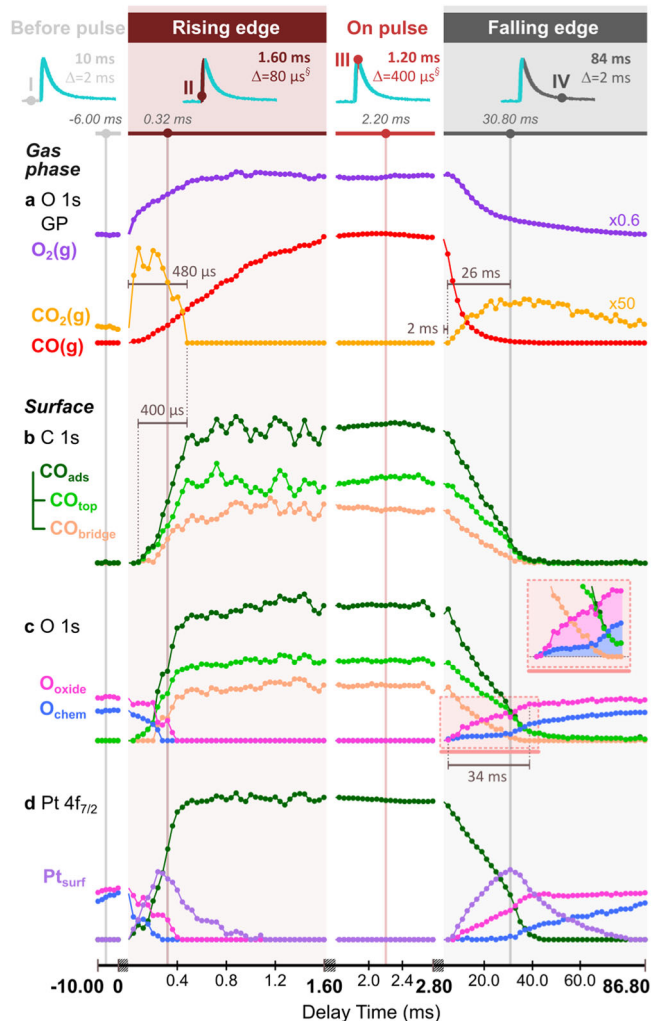
Fig. 3 | Areas trend data comparing gas phase and surface species in relevant core levels and across delay time in the CO oxidation of Pt(111) when pulsing CO at 10 Hz into a stream of O_2 gas. The analysis includes gas phase species determined from (**a**) O 1s core level, surface species as determined from (**b**) C 1s, (**c**) O 1s, and (**d**) Pt $4f_{7/2}$ spectra. **c** O 1s contains a red dashed box on the falling edge detailing a significant finding in the difference between chemisorbed oxygen (blue) and Pt surface oxide (pink) contributions. To effectively observe the evolution of all species throughout the reaction, different averaging of the spectra was required in each pulsing region as denoted at the top with or without a running average (§). Consequently, the noise level changes across pulsing regions. Physical breaks between pulsing regions are employed to help distinguish different regions. Particularly meaningful slices of time in each pulsing region are conveyed by guide lines with associated roman numerals (I–IV) whose fits can be found in the bottom panel of Fig. 2.

The most plausible explanation for the observed trends is that O_{chem} is the primary active species. The lack of O_{chem} signal alongside increasing O_{oxide} and CO_2 production on the falling edge is explained precisely by the high activity of O_{chem}, which is rapidly consumed to form CO_2 (Fig. 5). O_{oxide} begins to form when the *local* O_{chem} concentration exceeds 0.25–0.50 monolayers[58–62], appearing in patches of bare Pt where O_{chem} and CO_{ads} react. This less reactive O_{oxide} accumulates on the surface and can react with CO, as observed on the rising edge of the CO pulse, albeit at a lower rate[13,35,63,64]. When CO_2 production lags, the Pt_{surf} concentration decreases as O_{chem} increasingly occupies the surface, as observed in its enhanced signal. The system then moves toward a thermodynamically favored state with the stabilization of O_{oxide} shortly thereafter and little reactivity towards CO_2

conversion[58]. In agreement with these observations, the increased activity of O_{chem} causes larger oscillations compared to O_{oxide} during the 50 Hz experiment. Such a classical LH mechanism is supported by many experimental studies demonstrating the lack of O_{oxide} or its lower activity in the reaction[8–14]. This reaction was shown to predominantly occur on the terraces, with the step edges playing a minor role at the temperature used in the study[65–67]. While O_{oxide} is detected in large amounts on the active surface, O_{chem} drives the reaction, making it a minor yet crucial species due to its transient nature[68].

Nonetheless, the less reactive O_{oxide} likely contributes slightly to CO_2 conversion, as observed on the rising edge where O_{oxide} is consumed at a slower rate than O_{chem}. We propose a secondary CO oxidation mechanism involving O_{oxide}, consistent with presented experimental data and previous findings, such as those that have predicted higher activity *at the boundary* between the metallic (CO-covered) and oxide phases[34,69–75]. This mechanism requires the formation of individual PtO_4 clusters prior to the start of the catalytic reaction when the *local* oxygen coverage reaches 0.25–0.50 monolayers within bare Pt patches (as described earlier). Cluster formation has an estimated activation barrier of 0.44-0.82 eV from a pre-existing chain of O_{chem}[60] or three individual O_{chem}[50], respectively, comparable to O_{chem} diffusion (0.63 eV)[50] or phase-dependent CO_{ads} oxidation (0.49-1.01 eV)[13,64,76–79]. Further cluster growth into chains is hindered by a large activation barrier (1.13 eV)[50], allowing O_{chem} and O_{oxide} to coexist in close proximity until they react with CO_{ads}. Under the present experimental conditions of gas pressure, temperature, and exposure time, we can infer that we likely have a 4O-type[14] surface oxide (O_{oxide}) that coexists with O_{chem} on metallic Pt, based upon the expansive literature surrounding oxidation of Pt and identification via O *1s* and Pt 4f binding energies[80–84]. Bulk or surface α-PtO_2 trilayer oxide appear at a much higher binding energy of 73.5–74.1 eV and requires higher O_2 pressure and temperature[60,64,85,86]. In equilibrium, this oxide forms stripes with platinum atoms raised by 1.7 Å, each surrounded by four oxygen atoms, but likely beginning with smaller cluster-type structures similar to the PtO_4 clusters needed for the proposed reaction mechanism[58]. Pt_{surf} binding energy trends suggest the Pt surface transitions from a (111)-type surface to a more step-like structure (Supplementary Fig. 5). This supports the proposed dual mechanism: CO_{ads} initially reacts with O_{chem}, exposing bare Pt, but as O_{oxide} continues to grow, it dominates the reaction, leading to a stepped surface appearance. Furthermore, the diminished Pt_{surf} intensity with the stabilization of O_{oxide} may contribute to the lack of reactivity based upon the observed inactivity on a similar oxygen-terminated surface oxide on Rh(111) due to missing coordinately unsaturated sites[87] as compared to highly reactive PdO(101)[88] and RuO_2(110)[89] with available coordinately unsaturated sites.

The catalytic reaction starts when CO_{ads} abstracts a single oxygen atom from an individual oxide cluster to produce CO_2, a less activated step (0.1–0.3 eV)[64,66] than the reaction with O_{chem}. If the remaining partially reduced cluster is less reactive than *both* the initial cluster *and* O_{chem}, it remains stable until a O_{chem} atom attaches to the cluster, closing the catalytic cycle. This attachment is facile with a low activation energy (0.08–0.26 eV)[50], lower than the barrier for O_{chem} diffusion or reaction with CO_{ads}. For this reaction step, the availability of O_{chem} atoms in the immediate vicinity of the oxide is critical. The high reactivity of oxide clusters ensures bare Pt sites for O_2 dissociative adsorption, supplying O_{chem} directly next to the clusters. Thus, the most catalytically active surface for oxide clusters is composed of a largely CO-free Pt surface with numerous bare metallic Pt atoms readily available for O_2 adsorption and dissociation[90]. In CO-rich environments, the perimeter of partially reduced clusters remains CO-covered, preventing re-oxidation to a highly active state. Whereas O-rich environments promote the formation of thermodynamically stable but less active oxides, e.g. trilayer PtO_2. We also do not observe carbonate intermediates, theoretically predicted for direct oxidation of CO on trilayer
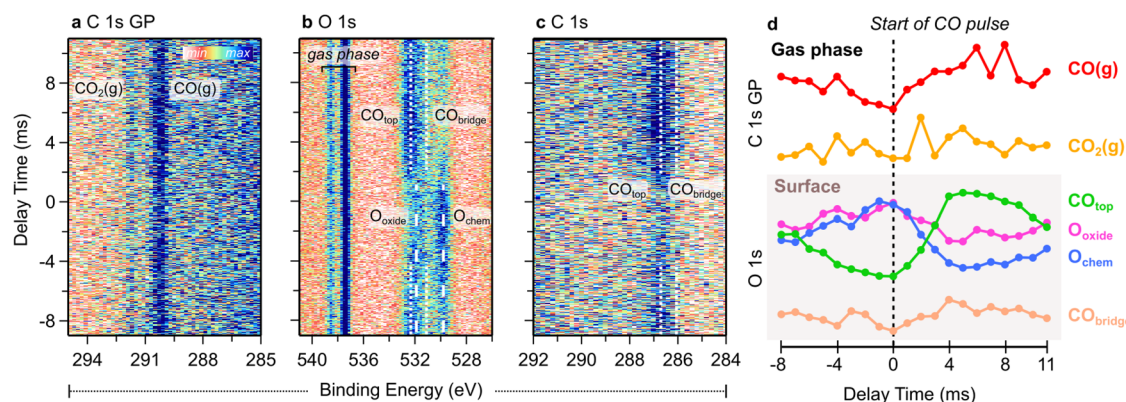
Fig. 4 | tr-APXPS of CO oxidation of Pt(111) when pulsing CO at 50 Hz into a stream of O_2 where CO_2 production can be controlled by tuning the pulsing parameters thus changing the surface-mediated response. Constant CO_2 production was achieved as shown in 2D plots of the **a** C *1s* GP, **b** O *1s*, and **c** C *1s* spectra, along with an analysis of **d** O *1s* intensity trends.
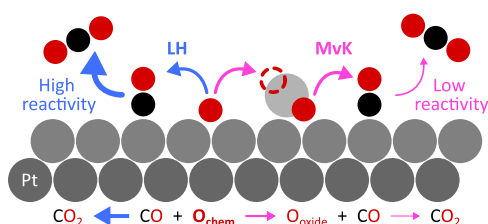

Fig. 5 | Proposed reactivity scheme of CO oxidation of Pt(111). High CO_2 production is emphasized upon reaction of CO_{ads} with O_{chem} as opposed to surface oxide O_{oxide}. O_{chem} primarily reacts with CO_{ads} to produce CO_2 (LH mechanism) but also forms O_{oxide}. In turn, O_{oxide} occasionally reacts with CO_{ads} to form CO_2 but is much less reactive than O_{chem} (MvK mechanism).

PtO_2 indicating that the surface oxide is not active[91–93]. The proposed difference in activity between a complete and partially reduced oxide cluster explains the discrepancy between the calculated activity of the 4O phase (O_{oxide}) and experimental findings, such as those by Miller et al.[14], which showed lower reactivity than O_{chem}. If only one of the two oxygen atoms in the 4 O phase is catalytically active, the overall reactivity of the phase will be limited by the abstraction of the second oxygen atom with potentially higher activation energy.

Moreover, the results reveal the chemical transformations behind the CO_2 spikes commonly detected at the start of oxidation/reduction pulses in a modulated gas feed, as used in industry[26,42,44,46]. Periodic modulations of the gas feed force the surface to oscillate between CO-poisoned and O-poisoned states, intermittently passing through the catalytically active phase described above. This also clarifies discrepancies in previous conflicting reports, where observations under steady-state conditions could favor different surface chemistry that does not capture transient species.

Altogether the optimized reaction conditions in this experiment concerning temperature, pressure, and CO/O_2 ratio provided the means to target a highly reactive state and bridge the pressure gap, as confirmed by the observation of a surface oxide. Altering these parameters would likely change the response of the catalyst by targeting different regions of the phase diagram with temperature and pressure changes. For example, a lower reaction temperature could lead to CO poisoning throughout the experiment, inhibiting oxygen adsorption, and prohibiting CO_2 production. Higher pressure could promote bulk oxide formation, likely accompanied by a different reaction mechanism than the current CO oxidation study involving chemisorbed oxygen and surface oxide. The initial CO/O_2 ratio has less of an effect on the reaction due in large part to our pulsing scheme where the CO/O_2 ratio is inherently changing throughout the CO pulse, constantly ramping over inactive and reactive states. We observe this effect in Supplementary Fig. 4 where the $CO_2(g)$ signal remains stable when changing the initial CO/O_2 ratio from 7.5/1 to 30/1.

In conclusion, the present tr-APXPS results suggest a primary LH mechanism involving O_{chem} as the active species with a secondary MvK mechanism concerning less reactive, largely spectator O_{oxide} clusters. The reaction takes place at specific instances during the CO pulse instigating open Pt areas for O_2 dissociation into reactive O_{chem} immediately consumed by a) CO_{ads} to produce CO_2 and b) formation of O_{oxide}. These observations offer new insights into the highly contested CO oxidation mechanism. The incorporation of both operando conditions and microsecond time resolution in tr-APXPS enabled the discovery of these highly active, transient species produced during surface transformations, facilitating the concurrent detection of reaction products, surface intermediates, and catalyst response. Even better time resolution could be possible in the future with a faster piezo valve to match the nanosecond time resolution of the DLD. We demonstrate how tuning pulsing parameters in periodic operation can optimize CO_2 formation, offering a valuable tool for improving catalytic technology designs.

The presented findings provide a strong motivation for revisiting the proposed mechanisms of some catalytic reactions; especially in cases when several distinct species can be attributed to the active component. Comparing the pathways of CO oxidation on hexagonal surfaces of other Pt-group metals is a natural next step. On the other hand, the time resolution is an additional benefit in chemical analysis of surfaces of novel catalytic materials.

Methods

Sample preparation and acquisition of time-resolved data

All experiments were performed at the HIPPIE beamline of the MAX IV Laboratory in Lund, Sweden[94]. Sample preparation took place on the solid-gas endstation (SGE). A Pt(111) single crystal mounted on a flag-style plate with a K-type thermocouple spot-welded to the sides of the crystal underwent two sputter (20 min at 1 kV and 10 mA emission current in 1×10^{-5} mbar Ar) and anneal (10 min at 600 °C) cycles. Pt was then transferred via air from SGE to the solid-liquid endstation of HIPPIE for tr-APXPS measurements where the backfilled chamber set-up has a routine base pressure of ~5×10^{-6} mbar when pumped with a 300 L turbomolecular pump. The endstation uses a SPECS PHOIBOS-NAP spectrometer equipped with a Surface Concepts 2D delay-line detector (DLD), which captures the arrival time of photoelectrons hitting its delay lines.

During the experiment, Pt(111) was kept at a reaction temperature of 333 ± 2 °C (as monitored by the thermocouple). The initial O_2 pressure of ~3.0×10^{-3} mbar burned away any residual carbon as verified by XPS. O_2 and CO gases had separate gas lines whose valves were

installed on the outside of the chamber with internal piping attached to the cone directed at the face of the sample (a few mm away). O_2 gas (N5.5 purity) was supplied via a mass flow controller set to 30 sccm throughout the experiment, resulting in a ~ 3.0×10^{-3} mbar pressure reading. CO gas (N3.7) was pulsed into the chamber via a Attotech GR020 piezo valve providing mbar internal pressure[56]. Note that the close proximity of the gas pipes at the front of the sample resulted in O_2 gas entering the CO pipe between CO gas pulses and was subsequently pushed out when pulsing as observed in an increase in O_2 gas phase signal (Figs. 2b and 3a). Gas attenuation may also play a role as photoelectrons will scatter less with CO than O_2 leading to an increase in O_2 signal with the introduction of CO. The operations of the piezo valve and the DLD were synchronized using a BNC 565 function generator (Fig. 1). The CO gas line contained a filter (PAL) to purify the gas and was constructed mainly from Cu pipe to minimize the well-known Ni carbonyl contaminates that form under elevated CO pressure upon reaction with stainless steel. The Ni 2p line was monitored continually throughout all experiments. The piezo valve required a constant back pressure of ~3 bar to ensure stable pulsing conditions. CO pulsing parameters varied depending on the experiment. Figures 2 and 3 and Supplementary Figs. 1, 2, and 5 represent datasets where the piezo valve was pulsed at 10 Hz under 240 V and 120 µs opening time. The pulsed data in Supplementary Fig. 4 were also recorded at 10 Hz, while varying the voltage (170–240 V) to obtain different O_2:CO ratios. Figure 4 and Supplementary Fig. 3 show datasets where the piezo valve was pulsed at 50 Hz, 160 V, and 53 µs vs. 170 V and 250 µs, respectively.

Using a special measurement mode in the SPECS Prodigy software connected to the timing hardware in the analyzer and external synchronization of CO gas pulses with the DLD provided the means to acquire time-resolved data while sweeping over kinetic energy channels to acquire 2D plots of binding energy vs. time. The time axis was derived from the CO pulsing frequency and number of time channels: CO pulsing at 10 Hz and 2500 channels provided a 100 ms time window with 40 µs time resolution, whereas CO pulsing at 50 Hz and 500 channels provided a 20 ms time window with 40 µs time resolution. While our previous studies[56] used a simple pump-probe measurement scheme measuring one delay at a time, we measured all delays simultaneously with the upgraded detection scheme from camera to DLD (Fig. 1b).

Core levels of interest included the O $1s$ (hv = 750 eV), C $1s$ (750 eV), and Pt 4 f (260 eV) lines, recorded at a pass energy of 100 eV with a 0.8 mm analyzer slit. O $1s$ and C $1s$ spectra were acquired at both gas phase and surface positions, whereas the Pt 4f line was measured only in the surface position. As adsorbed CO is always located on the surface, we did not tune the photon energy to be surface-sensitive for acquiring C $1s$ spectra. The surface position describes the typical XPS sample position 300 µm away from the analyzer cone (cone diameter 300 µm). The gas phase position is 450 µm from the standard XPS position; here, only gas phase species are detected. Note that the APXPS detection of gas phase species is better than conventional mass spectrometry (MS): First of all, it benefits from the synchronization of gas injections and high time resolution of the DLD. Secondly, it probes the local gas composition in the near vicinity of the sample surface (as detailed in Supplementary Fig. 6 of Küst et al.[95]). Therefore, MS data was not recorded in the present study. The beamline exit slit was open to 50 µm at the surface position and, 100 µm and 200 µm for O $1s$ and C $1s$ gas phase positions, respectively.

Data analysis

tr-APXPS data was analyzed in IgorPro (WaveMetrics) and fitted using the EccentricXPS procedure. Each 2D plot was energy-calibrated against the Fermi level. Linear, Shirley, and polynomial background subtractions were administered depending on the core level and sample location. All gas phase spectra (O $1s$, C $1s$) required a linear background subtraction. Pt $4f$ and C $1s$ spectra required Shirley

background subtraction. Deviating from that general procedure, a linear background was subtracted from the C $1s$ spectra when the CO adsorbate signal was not detected (i.e., before and after the CO pulse). The O $1s$ line required additional care due to its close proximity to the Pt $4p_{3/2}$ level, necessitating a fourth-order polynomial fit to accurately approximate the tail of the Pt feature. In the presence of high-pressure CO from the CO pulse, a Shirley background subtraction was necessary before the polynomial background subtraction. Post background subtraction, all spectra were fit with Voigt peak shapes compounded with an asymmetric factor when needed, e.g., Pt $4f$ bulk and surface features. All Pt $4f$ spectra were intensity normalized by the total Pt peak area.

Further processing of tr-APXP spectra included averaging spectra differently in the four pulsing regions to achieve a reasonable signal-to-noise ratio while preserving relevant time information. For instance, the rising edge contains essential information about the surface response when the CO pulse is first introduced, requiring minimal averaging to capture compositional changes within this short time-frame, i.e., 80 µs averaging over 2 spectra. Conversely, the falling edge has a slower response time due to the dependence of CO removal on pumping speed, leading to 2 ms averaging over 50 spectra for the 10 Hz dataset. The before-pulse region followed the same treatment as the falling edge since it is the tail of the falling edge, whereas the on-pulse region required averaging over 400 µs/10 spectra for the 10 Hz dataset. A running average with a step of 1 was also performed on the rising edge and on-pulse spectra to ensure all reaction intermediates were captured with sufficient time resolution. Note that the 50 Hz dataset required averaging over 1 ms/50 spectra to achieve a reasonable signal-to-noise ratio for fitting. All fitting parameters can be found in Supplementary Table 3.

Comparison between pulsing and flow experiments

CO pulsing vs. flow experiments required adjusting either the CO mass flow controller (4 sccm) or CO pulsing voltage (170–240 V), respectively, to achieve the targeted CO:O_2 ratios, while O_2 remained at 30 sccm output throughout the experiments and the system heated to 333 °C. While monitoring the response of CO(g) in C $1s$, the CO pulsing voltage was adjusted to match the intensity of the CO(g) peak measured in the flow experiment, thus ensuring the same CO:O_2 ratio when pulsing. All spectra were collected in time-resolved mode and integrated to produce the line spectra presented in Supplementary Fig. 4.

Data availability

The XPS data generated in this study have been deposited in the Figshare database [https://doi.org/10.6084/m9.figshare.28067600].

References

1.   Wintterlin, J., Völkening, S., Janssens, T. V. W., Zambelli, T. & Ertl, G. Atomic and macroscopic reaction rates of a surface-catalyzed reaction. *Science* **278**, 1931–1934 (1997).
2.   Campbell, C. T., Ertl, G., Kuipers, H. & Segner, J. A molecular beam study of the adsorption and desorption of oxygen from a Pt(111) surface. *Surf. Sci.* **107**, 220–236 (1981).
3.   Bär, M., Zülicke, C., Eiswirth, M. & Ertl, G. Theoretical modeling of spatiotemporal self-organization in a surface catalyzed reaction exhibiting bistable kinetics. *J. Chem. Phys.* **96**, 8595–8604 (1992).
4.   Hendriksen, B. L. M. & Frenken, J. W. M. CO oxidation on Pt(110): scanning tunneling microscopy inside a high-pressure flow reactor. *Phys. Rev. Lett.* **89**, 046101 (2002).
5.   Carlsson, P. A. et al. A transient in situ FTIR and XANES study of CO oxidation over Pt/Al 2 O 3 catalysts. *J. Catal.* **226**, 422–434 (2004).
6.   Singh, J. et al. Generating highly active partially oxidized platinum during oxidation of carbon monoxide over Pt/Al2O3: in situ, time-resolved, and high-energy-resolution X-ray absorption. *Spectroscopy. Angew. Chemie Int. Ed.* **47**, 9260–9264 (2008).

7.   van Spronsen, M. A., Frenken, J. W. M. & Groot, I. M. N. Surface science under reaction conditions: CO oxidation on Pt and Pd model catalysts. *Chem. Soc. Rev.* **46**, 4347–4374 (2017).

8.   Newton, M. A. & Bravo-Suarez, J. J. Time resolved operando X-ray techniques in catalysis, a case study: CO oxidation by O2 over Pt surfaces and alumina supported Pt catalysts. *Catalysts* **7**, 58 (2017).

9.   Chung, J. Y. et al. In-situ study of the catalytic oxidation of CO on a Pt(1 1 0) surface using ambient pressure X-ray photoelectron spectroscopy. *Surf. Sci.* **603**, L35–L38 (2009).

10. Calderón, S. K. et al. CO oxidation on Pt(111) at near ambient pressures. *J. Chem. Phys.* **144**, 044706 (2016).

11. Schnadt, J. et al. The new ambient-pressure X-ray photoelectron spectroscopy instrument at MAX-lab. *J. Synchrotron Radiat.* **19**, 701–704 (2012).

12. Chen, M. S. et al. Highly active surfaces for CO oxidation on Rh, Pd, and Pt. *Surf. Sci.* **601**, 5326–5331 (2007).

13. Gao, F. et al. CO oxidation trends on Pt-group metals from ultrahigh vacuum to near atmospheric pressures: a combined in situ PM-IRAS and reaction kinetics study. *Surf. Sci.* **603**, 65–70 (2009).

14. Miller, D. et al. Different reactivity of the various platinum oxides and chemisorbed oxygen in CO oxidation on Pt(111). *J. Am. Chem. Soc.* **136**, 6340–6347 (2014).

15. Szlachetko, J. et al. Subsecond and in situ chemical speciation of Pt/ Al2O3 during oxidation-reduction cycles monitored by high-energy resolution off-resonant x-ray spectroscopy. *J. Am. Chem. Soc.* **135**, 19071–19074 (2013).

16. Gänzler, A. M. et al. Unravelling the different reaction pathways for low temperature CO oxidation on Pt/CeO2 and Pt/Al2O3 by spatially resolved structure-activity correlations. *J. Phys. Chem. Lett.* **10**, 7698–7705 (2019).

17. Gao, F. & Goodman, D. W. Reaction kinetics and polarization modulation infrared reflection absorption spectroscopy investigations of CO oxidation over planar Pt-group model catalysts. *Langmuir* **26**, 16540–16551 (2010).

18. Kalz, K. F. et al. Future challenges in heterogeneous catalysis: understanding catalysts under dynamic reaction conditions. *ChemCatChem* **9**, 17–29 (2017).

19. Meirer, F. & Weckhuysen, B. M. Spatial and temporal exploration of heterogeneous catalysts with synchrotron radiation. *Nat. Rev. Mater.* **3**, 324–340 (2018).

20. Shetty, M. et al. The catalytic mechanics of dynamic surfaces: stimulating methods for promoting catalytic resonance. *ACS Catal.* **10**, 12666–12695 (2020).

21. Chavez, S. et al. Studying, promoting, exploiting, and predicting catalyst dynamics: the next frontier in heterogeneous catalysis. *J. Phys. Chem. C* **127**, 2127–2146 (2023).

22. Maeda, N., Meemken, F., Hungerbühler, K. & Baiker, A. Spectroscopic detection of active species on catalytic surfaces: steady-state versus transient method. *Chimia* **66**, 664 (2012).

23. Campbell, C. T. The degree of rate control: a powerful tool for catalysis research. *ACS Catal.* **7**, 2770–2779 (2017).

24. Armstrong, C. D. & Teixeira, A. R. Advances in dynamically controlled catalytic reaction engineering. *React. Chem. Eng.* **5**, 2185–2203 (2020).

25. Zhang, Z., Zandkarimi, B. & Alexandrova, A. N. Ensembles of metastable states govern heterogeneous catalysis on dynamic interfaces. *Acc. Chem. Res.* **53**, 447–458 (2020).

26. Shavorskiy, A., Schnadt, J. & Knudsen, J. Time resolved ambient pressure X-ray photoelectron spectroscopy. *ACS Symp. Ser.* **1396**, 219–248 (2021).

27. Roger, M. et al. Improving time-resolution and sensitivity of in situ X-ray photoelectron spectroscopy of a powder catalyst by modulated excitation. *Chem. Sci.* **14**, 7482–7491 (2023).

28. Morgan, K. et al. Forty years of temporal analysis of products. *Catal. Sci. Technol.* **7**, 2416–2439 (2017).

29. Gleaves, J. T., Ebner, J. R. & Kuechler, T. C. Temporal analysis of products (TAP)—a unique catalyst evaluation system with sub-millisecond time resolution. *Catal. Rev. Sci. Eng.* **30**, 49–116 (1988).

30. Libuda, J. & Freund, H. J. Molecular beam experiments on model catalysts. *Surf. Sci. Rep.* **57**, 157–298 (2005).

31. Libuda, J. Reaction kinetics on model catalysts: molecular beam methods and time-resolved vibrational spectroscopy. *Surf. Sci.* **587**, 55–68 (2005).

32. Ledesma, C., Yang, J., Chen, D. & Holmen, A. Recent approaches in mechanistic and kinetic studies of catalytic reactions using SSITKA technique. *ACS Catal.* **4**, 4527–4547 (2014).

33. BENNETT, C. O. Understanding heterogeneous catalysis through the transient method. 1–32 https://doi.org/10.1021/BK-1982-0178. CH001 (1982).

34. Ferri, D., Newton, M. A. & Nachtegaal, M. Modulation excitation X-ray absorption spectroscopy to probe surface species on heterogeneous catalysts. *Top. Catal.* **54**, 1070–1078 (2011).

35. Ferri, D. et al. First steps in combining modulation excitation spectroscopy with synchronous dispersive EXAFS/DRIFTS/mass spectrometry for in situ time resolved study of heterogeneous catalysts. *Phys. Chem. Chem. Phys.* **12**, 5634–5646 (2010).

36. Ibraliu, A. et al. Tracking minority species in redox reactions: a quantitative combined XAS and modulation excitation study. *Angew. Chemie Int. Ed.* e202401888 https://doi.org/10.1002/ANIE. 202401888 (2024).

37. Buttignol, F., Maggiulli, L., Kochetygov, I., Alxneit, I. & Ferri, D. Operando spectroscopy of catalysts exploiting multi-technique and modulated excitation approaches. *Chimia* **78**, 313–319 (2024).

38. Knudsen, J. et al. Catalysis in frequency space: resolving hidden surface structure and activity oscillations. https://doi.org/10.21203/ RS.3.RS-4242040/V1 (2024).

39. Guo, M., Dongfang, N., Iannuzzi, M., van Bokhoven, J. A. & Artiglia, L. Structure and reactivity of active oxygen species on silver surfaces for ethylene epoxidation. *ACS Catal.* **14**, 10234–10244 (2024).

40. Schüth, F., Henry, B. E. & Schmidt, L. D. Oscillatory reactions in heterogeneous catalysis. *Adv. Catal.* **39**, 51–127 (1993).

41. Yokota, K., Muraki, H. & Fujitani, Y. Rh-Free Three-way catalysts for automotive exhaust control. in *SAE Technical Papers 850129* (SAE International, 1985).

42. Gänzler, A. M. et al. Operando spatially and time-resolved X-ray absorption spectroscopy and infrared thermography during oscillatory CO oxidation. *J. Catal.* **328**, 216–224 (2015).

43. Hodonj, D. et al. Impact of operation parameters and lambda input signal during lambda-dithering of three-way catalysts for low-temperature performance enhancement. *Appl. Catal. B Environ. Energy* **345**, 123657 (2024).

44. Gänzler, A. M. et al. Operando X-ray absorption spectroscopy study during conditioning of Pt-based catalysts and its implications for CO oxidation. *J. Phys. Chem. C* **124**, 20090–20100 (2020).

45. Muraki, H., Sobukawa, H. & Fujitani, Y. Dynamic behavior of automotive noble metal catalysts in model gas systems. *Nippon Kagaku Kaishi* **1986**, 532–537 (1986).

46. Lott, P., Casapu, M., Grunwaldt, J. D. & Deutschmann, O. A review on exhaust gas after-treatment of lean-burn natural gas engines—from fundamentals to application. *Appl. Catal. B Environ.* **340**, 123241 (2024).

47. Schramm, H., Kienle, A., Kaspereit, M. & Seidel-Morgenstern, A. Improved operation of simulated moving bed processes through cyclic modulation of feed flow and feed concentration. *Chem. Eng. Sci.* **58**, 5217–5227 (2003).

48. Silveston, P. L. & Hudgins, R. R. Periodic pressure forcing of catalytic reactions. *Chem. Eng. Sci.* **59**, 4055–4064 (2004).

49. Shamim, T. & Medisetty, V. G. Dynamic response of automotive catalytic converters to variations in air-fuel ratio. *J. Eng. Gas Turbines Power* **125**, 547–554 (2003).

50. Ardagh, M. A., Abdelrahman, O. A. & Dauenhauer, P. J. Principles of dynamic heterogeneous catalysis: surface resonance and turnover frequency response. *ACS Catal.* **9**, 6929–6937 (2019).

51. Swartz, C. L. E. & Kawajiri, Y. Design for dynamic operation—a review and new perspectives for an increasingly dynamic plant operating environment. *Comput. Chem. Eng.* **128**, 329–339 (2019).

52. Fischer, K. L. & Freund, H. On the optimal design of load flexible fixed bed reactors: integration of dynamics into the design problem. *Chem. Eng. J.* **393**, 124722 (2020).

53. Stankiewicz, A. & Kuczynski, M. An industrial view on the dynamic operation of chemical converters. *Chem. Eng. Process. Process Intensif.* **34**, 367–377 (1995).

54. Knudsen, J. et al. Stroboscopic operando spectroscopy of the dynamics in heterogeneous catalysis by event-averaging. *Nat. Commun.* **12**, 1–8 (2021).

55. Boix, V. et al. Following the kinetics of undercover catalysis with APXPS and the role of hydrogen as an intercalation promoter. *ACS Catal.* **12**, 9897–9907 (2022).

56. Shavorskiy, A. et al. Gas pulse-X-ray probe ambient pressure photoelectron spectroscopy with submillisecond time resolution. *ACS Appl. Mater. Interfaces* **13**, 47629–47641 (2021).

57. Golibrzuch, K. et al. CO desorption from a catalytic surface: elucidation of the role of steps by velocity-selected residence time measurements. *J. Am. Chem. Soc.* **137**, 1465–1475 (2015).

58. Xu, J., Xie, W., Han, Y. & Hu, P. Atomistic insights into the oxidation of flat and stepped platinum surfaces using large-scale machine learning potential-based grand-canonical Monte Carlo. *ACS Catal.* **12**, 14812–14824 (2022).

59. Devarajan, S. P., Hinojosa, J. A. & Weaver, J. F. STM study of high-coverage structures of atomic oxygen on Pt(1 1 1): p(2 × 1) and Pt oxide chain structures. *Surf. Sci.* **602**, 3116–3124 (2008).

60. Fantauzzi, D. et al. Growth of stable surface oxides on Pt(111) at near-ambient pressures. *Angew. Chemie Int. Ed.* **56**, 2594–2598 (2017).

61. Hawkins, J. M., Weaver, J. F. & Asthagiri, A. Density functional theory study of the initial oxidation of the Pt(111) surface. *Phys. Rev. B Condens. Matter Mater. Phys.* **79**, 125434 (2009).

62. Miller, D. J. et al. Oxidation of Pt(111) under near-ambient conditions. *Phys. Rev. Lett.* **107**, 195502 (2011).

63. Butcher, D. R. et al. In situ oxidation study of Pt(110) and its interaction with CO. *J. Am. Chem. Soc.* **133**, 20319–20325 (2011).

64. Farkas, A. et al. High pressure carbon monoxide oxidation over platinum (111). *J. Phys. Chem. C* **117**, 9932–9942 (2013).

65. Neugebohren, J. et al. Velocity-resolved kinetics of site-specific carbon monoxide oxidation on platinum surfaces. *Nature* **558**, 280–283 (2018).

66. Matsushima, T., Ohno, Y. & Rar, A. Reaction sites for carbon monoxide oxidation on a stepped platinum (112) surface: a spatial distribution study of product desorption. *Surf. Sci.* **293**, 145–151 (1993).

67. Urakawa, A., Bürgi, T., Schläpfer, H. P. & Baiker, A. Simultaneous in situ monitoring of surface and gas species and surface properties by modulation excitation polarization-modulation infrared reflection-absorption spectroscopy: CO oxidation over Pt film. *J. Chem. Phys.* **124**, 54717 (2006).

68. Makeev, A. G., Slinko, M. M. & Luss, D. Mathematical modeling of oscillating CO oxidation on Pt-group metals at near atmospheric pressure: activity of metallic and oxidized surfaces. *Appl. Catal. A Gen.* **571**, 127–136 (2019).

69. Li, W. X. & Hammer, B. Reactivity of a gas/metal/metal-oxide three-phase boundary: CO oxidation at the Pt(1 1 1)–c(4 × 2)–2CO/α-PtO2 phase boundary. *Chem. Phys. Lett.* **409**, 1–7 (2005).

70. Wang, J. G. et al. One-dimensional PtO2 at Pt steps: formation and reaction with CO. *Phys. Rev. Lett.* **95**, 256102 (2005).

71. Pedersen, T. M., Xue Li, W. & Hammer, B. Structure and activity of oxidized Pt(110) and α-PtO2. *Phys. Chem. Chem. Phys.* **8**, 1566–1574 (2006).

72. Singh, J., Nachtegaal, M., Alayon, E. M. C., Stötzel, J. & Van Bokhoven, J. A. Dynamic structure changes of a heterogeneous catalyst within a reactor: oscillations in CO oxidation over a supported platinum catalyst. *ChemCatChem* **2**, 653–657 (2010).

73. Albinsson, D. et al. Shedding light on CO oxidation surface chemistry on single Pt catalyst nanoparticles inside a nanofluidic model pore. *ACS Catal.* **11**, 2021–2033 (2021).

74. Balmes, O., Prevot, G., Torrelles, X., Lundgren, E. & Ferrer, S. Generation of surface steps on Pt(9 7 7) induced by the catalytic oxidation of CO. *J. Catal.* **309**, 33–37 (2014).

75. Johánek, V. et al. High low-temperature CO oxidation activity of platinum oxide prepared by magnetron sputtering. *Appl. Surf. Sci.* **345**, 319–328 (2015).

76. Alavi, A., Hu, P., Deutsch, T., Silvestrelli, P. L. & Hutter, J. CO oxidation on Pt(111): an ab initio density functional theory study. *Phys. Rev. Lett.* **80**, 3650 (1998).

77. Eichler, A. C. O. Oxidation on transition metal surfaces: reaction rates from first principles. *Surf. Sci.* **498**, 314–320 (2002).

78. Liu, Z. P. & Hu, P. General trends in the barriers of catalytic reactions on transition metal surfaces. *J. Chem. Phys.* **115**, 4977–4980 (2001).

79. Burnett, D. J. et al. In-situ soft X-ray studies of CO oxidation on the Pt(1 1 1) surface. *Surf. Sci.* **564**, 29–37 (2004).

80. Hecq, M., Hecq, A., Delrue, J. P. & Robert, T. Sputtering deposition, XPS and X-ray diffraction characterization of oxygen-platinum compounds. *J. Less Common Met.* **64**, P25–P37 (1979).

81. Held, G., Jones, L. B., Seddon, E. A. & King, D. A. Effect of oxygen adsorption on the chiral Pt{531} surface. *J. Phys. Chem. B* **109**, 6159–6163 (2005).

82. Légaré, P. et al. On the interaction of O2 with Pt(111) and Pt(557) surfaces: core-level shift study using conventional and synchrotron radiation sources. *Surf. Sci.* **198**, 69–78 (1988).

83. Ono, L. K., Yuan, B., Heinrich, H. & Roldan Cuenya, B. Formation and thermal stability of platinum oxides on size-selected platinum nanoparticles: support effects. *J. Phys. Chem. C* **114**, 22119–22133 (2010).

84. Kuribayashi, K. & Kitamura, S. Preparation of Pt-PtOx thin films as electrode for memory capacitors. *Thin Solid Films* **400**, 160–164 (2001).

85. Ellinger, C., Stierle, A., Robinson, I. K., Nefedov, A. & Dosch, H. Atmospheric pressure oxidation of Pt(111). *J. Phys. Condens. Matter* **20**, 184013 (2008).

86. Seriani, N., Pompe, W. & Ciacchi, L. C. Catalytic oxidation activity of Pt3O4 surfaces and thin films. *J. Phys. Chem. B* **110**, 14860–14869 (2006).

87. Lundgren, E. et al. The surface oxide as a source of oxygen on Rh(1 1 1). *J. Electron Spectros. Relat. Phenomena* **144–147**, 367–372 (2005).

88. Gustafson, J. et al. The role of oxides in catalytic CO oxidation over rhodium and palladium. *ACS Catal.* **8**, 4438–4445 (2018).

89. Over, H., Seitsonen, A. P., Lundgren, E., Schmid, M. & Varga, P. Direct imaging of catalytically important processes in the oxidation of CO over RuO2(110) [6]. *J. Am. Chem. Soc.* **123**, 11807–11808 (2001).

90. Garcia-Martinez, F. et al. Catalytic oxidation of CO on a curved Pt(111) surface: simultaneous ignition at all facets through a transient CO-O complex. *Angew. Chemie Int. Ed.* 59, 20037–20043 (2020).

91. Ackermann, M. D. et al. Structure and reactivity of surface oxides on Pt(110) during catalytic CO oxidation. *Phys. Rev. Lett.* **95**, 255505 (2005).

92. Newton, M. A., Ferri, D., Smolentsev, G., Marchionni, V. & Nachtegaal, M. Room-temperature carbon monoxide oxidation by oxygen over Pt/Al2O3 mediated by reactive platinum carbonates. *Nat. Commun. 2015* **61**, 1–7 (2015).

93. Gong, X. Q., Raval, R. & Hu, P. General insight into CO oxidation: a density functional theory study of the reaction mechanism on platinum oxides. *Phys. Rev. Lett.* **93**, 106104 (2004).

94. Zhu, S. et al. HIPPIE: a new platform for ambient-pressure X-ray photoelectron spectroscopy at the MAX IV laboratory. *J. Synchrotron Radiat.* **28**, 624–636 (2021).

95. Küst, U. et al. Temperature-dependent selectivity and detection of hidden carbon deposition in methane oxidation. *ACS Catal.* **14**, 5978–5986 (2024).

Author contributions

C.N.E. acquired the data, analyzed and interpreted the results, and drafted and revised the manuscript. W.W. designed and built the experimental hardware and acquired the data. U.K. and J.P. acquired the data and drafted the manuscript. R.H.T. and M.S. supported the experiments and drafted the manuscript. J.S. drafted the manuscript. J.K. designed the experiment, acquired the data, and drafted and revised the manuscript. A.S. designed the experiment, acquired the data, interpreted the results, and drafted and revised the manuscript.

Competing interests

The authors declare no competing interests.

Additional information

Supplementary information The online version contains supplementary material available at https://doi.org/10.1038/s41467-025-56576-5.

Correspondence and requests for materials should be addressed to Andrey Shavorskiy.

Peer review information *Nature Communications* thanks the anonymous reviewers for their contribution to the peer review of this work. A peer review file is available.

Reprints and permissions information is available at http://www.nature.com/reprints

Publisher's note Springer Nature remains neutral with regard to jurisdictional claims in published maps and institutional affiliations.